THE JOURNAL OF BIOLOGICAL CHEMISTRY Vol. 278, No. 12, Issue of March 21, pp. 10842–10850, 2003
Printed in U.S.A.

Congo Red Populates Partially Unfolded States of an Amyloidogenic Protein to Enhance Aggregation and Amyloid Fibril Formation*

Received for publication, December 9, 2002, and in revised form, January 9, 2003
Published, JBC Papers in Press, January 15, 2003, DOI 10.1074/jbc.M212540200

Yong-Sung Kim‡§, Theodore W. Randolph¶, Mark C. Manning‡, Fred J. Stevens‖, and John F. Carpenter‡**

From the ‡Department of Pharmaceutical Sciences, School of Pharmacy, University of Colorado Health Sciences Center, Denver, Colorado 80262, the ¶Department of Chemical Engineering, University of Colorado, Boulder, Colorado 80309, and the ‖Bioscience Division, Argonne National Laboratory, Argonne, Illinois 60439

Congo red (CR) has been reported to inhibit or enhance amyloid fibril formation by several proteins. To gain insight into the mechanism(s) for these apparently paradoxical effects, we studied as a model amyloidogenic protein, a dimeric immunoglobulin light chain variable domain. With a range of molar ratios of CR, *i.e.* r = [CR]/[protein dimer], we investigated the aggregation kinetics, conformation, hydrogen-deuterium exchange, and thermal stability of the protein. In addition, we used isothermal titration calorimetry to characterize the thermodynamics of CR binding to the protein. During incubation at 37 °C or during thermal scanning, with CR at r = 0.3, 1.3, and 4.8, protein aggregation was greatly accelerated compared with that measured in the absence of the dye. In contrast, with CR at r = 8.8, protein unfolding was favored over aggregation. The aggregates formed with CR at r = 0 or 0.3 were typical amyloid fibrils, but mixtures of amyloid fibrils and amorphous aggregates were formed at r = 1.3 and 4.8. CR decreased the apparent thermal unfolding temperature of the protein. Furthermore, CR perturbed the tertiary structure of the protein without significantly altering its secondary structure. Consistent with this result, CR also increased the rate of hydrogen-deuterium exchange by the protein. Isothermal titration calorimetry showed that CR binding to the protein was enthalpically driven, indicating that binding was mainly the result of electrostatic interactions. Overall, these results demonstrate that at low concentrations, CR binding to the protein favors a structurally perturbed, aggregation-competent species, resulting in acceleration of fibril formation. At high CR concentration, protein unfolding is favored over aggregation, and fibril formation is inhibited. Because low concentrations of CR can promote amyloid fibril formation, the therapeutic utility of this compound or its analogs to inhibit amyloidoses is questionable.

Amyloidoses are protein misfolding disorders in which soluble proteins aggregate to form insoluble fibrils, accumulation of which has been implicated in several diseases, such as Alzheimer's, Parkinson's, and Huntington's diseases, and systemic amyloidoses (1, 2). Numerous *in vitro* studies have supported the thesis that partially folded protein molecules are the precursors for the nucleation and growth of amyloid fibrils (1, 3), even though the detailed molecular mechanism underlying fibril formation is not well defined. However, it is well established that thermodynamic and conformational stability of native proteins, which are determined by intrinsic or extrinsic factors, are inversely related to their propensity to form amyloid fibrils (4–7). Therefore substantial efforts have been made to discover ligands (which could be used to treat or prevent amyloidoses) that can strongly bind to and stabilize the fully folded, native state of proteins, resulting in inhibition of fibril formation (*e.g.* 8).

Congo red (CR)[1] has been the subject of several studies investigating its effects on the formation of fibrils (*e.g.* 9–13) and is often used diagnostically as a stain for amyloid fibrils (2). CR is a symmetrical sulfonated azodye with a hydrophobic center consisting of a biphenyl group spaced between the negatively charged sulfate groups. CR binds to amyloid fibrils to induce a characteristic shift in maximal absorbance from ~490 to ~540 nm and an enhanced apple-green birefringence and dichroism under polarized light (14–16). The binding mechanism has been proposed to be intercalation of CR molecules between the antiparallel β-pleated sheets of amyloid fibrils by aromatic stacking (14, 15, 17, 18) or alignment of CR molecules along the fibril axes by electrostatic interactions between the negatively charged sulfate groups of CR and the positively charged amino acid residues of proteins (16, 19).

CR has been reported to stabilize Aβ monomer and to inhibit its oligomerization (20), to inhibit the structural conversion of normal prion protein into its aggregation-competent pathogenic form (9, 10), and to reduce Aβ-amyloid neurotoxicity by binding to preformed fibrils (21). Because of these findings, CR and its analogs have been screened as potential therapeutic inhibitors of amyloid fibril formation (11, 12). However, although CR at high concentrations inhibited amyloid fibril formation by Aβ-peptides (13) and prion proteins (12), at lower levels CR accelerated fibril formation. Also, the binding of CR to some proteins induces formation of soluble oligomers (22, 23), which could be precursors of fibrils. Thus, even the phenomenological effects of CR on protein aggregation and fibril-

* This work was supported by National Science Foundation Grant BES 0138595 (to T. R. W. and J. F. C.). The costs of publication of this article were defrayed in part by the payment of page charges. This article must therefore be hereby marked "*advertisement*" in accordance with 18 U.S.C. Section 1734 solely to indicate this fact.

§ Present address: Dept. of Chemical Engineering, Massachusetts Institute of Technology, Cambridge, MA 02139.

** To whom correspondence should be addressed: Center for Pharmaceutical Biotechnology, University of Colorado Health Sciences Center, 4200 East 9th Ave., Denver, CO 80262. Tel.: 303-315-6075; Fax: 303-315-6281; E-mail: John.Carpenter@uchsc.edu.

[1] The abbreviations used are: CR, Congo red; FT-IR, Fourier transform infrared; GAGs, glycosaminoglycans; HX, hydrogen-deuterium exchange; IR, infrared; ITC, isothermal titration calorimetry; SEC, size exclusion high performance liquid chromatography; TEM, transmission electron microscopy; ThT, thioflavin T; V_L, immunoglobulin light chain variable domain.

logenesis appear to be highly variable, and the mechanism(s) underlying these differences have not been determined.

There have been studies that document CR binding to native or partially folded states of several different proteins, regardless of their secondary structures (9, 14, 22–28). However, there have not been any detailed reports on the effects of CR binding on protein conformation nor on the potential roles that binding-induced structural changes might play in modulation of protein fibrillization by CR. In addition, the driving forces of CR binding to proteins remain controversial, as to whether the binding is caused by hydrophobic interactions, electrostatic interactions, or both (18, 23, 27, 28).

Recently we showed that CR enhanced amyloid fibril formation by an amyloidogenic immunoglobulin light chain variable domain (V_L), SMA, under high pressure (29). In the present study, to gain further insight into the mechanism(s) for CR effects on amyloid fibril formation, we characterized (at atmospheric pressure) the aggregation kinetics, conformational changes, and thermal stability of SMA with a range of molar ratios of CR. In addition, we used isothermal titration calorimetry to study the thermodynamics of CR binding to SMA.

EXPERIMENTAL PROCEDURES

Materials—Recombinant V_L SMA was expressed in *Escherichia coli* and purified by the methods of Wilkins-Stevens *et al.* (30) and Raffen *et al.* (5) with the following modifications. Instead of 5-ml prepacked Econo-Pac Q and S cartridges, High Q and S resins (Bio-Rad) were packed in 1 × 50-cm glass columns (Bio-Rad). Fractions were eluted with an 8× volume (400 ml), 0–900 mM NaCl gradient, collected, and assayed by SDS-PAGE. The fractions containing the protein were pooled and concentrated to 15–20 mg/ml with a stirred ultracentrifuge cell (Amicon) and a YM3 membrane (Amicon). All purification procedures were performed at 4 °C. The purity of the protein exceeded 99% based on SDS-PAGE analysis. The purified protein was stored at 4 °C in 10 mM potassium phosphate, pH 7.4, plus 100 mM NaCl buffer (5, 7, 30). The SMA concentration was estimated using an extinction coefficient of 1.71 mg ml^{-1} cm^{-1} at 280 nm (30). Recombinant SMA has the same sequence as the V_L that originated from lymph node-derived amyloid fibrils of a patient with immunoglobulin light chain-related amyloidosis (30). SMA is a homodimer with a dimerization constant of 7×10^5 M^{-1} (0.054 mg/ml) (30). The SMA molar concentration was calculated using a dimer molecular mass of 25.5 kDa because the protein dominantly exists as a dimer under the experimental concentrations used in the present study.

Throughout the experiments, 10 mM potassium phosphate, pH 7.4, plus 100 mM NaCl buffer ("buffer") was used. CR (Sigma C6767) solutions were prepared daily in buffer and filtered three times using a 0.45-μm pore size polysulfone filter (Whatman) (29). The CR concentration was determined using an extinction coefficient of 5.93×10^4 M cm^{-1} at 505 nm after dilution into 40% (v/v) ethanol water (16). Other chemicals were of reagent or higher grade.

Aggregation of SMA with Various Molar Ratios of CR with Agitation—Solutions of 40 μM (1 mg/ml) SMA with various molar ratios of CR (r = [CR]/[SMA dimer]), *i.e.* r = 0, 0.3, 1.3, 4.8, and 8.8, were incubated in buffer, containing 0.05% NaN_3, at 37 °C with agitation at 250 rpm in an orbital shaker (6, 7). After centrifugation of the samples (14,000 rpm for 5 min), the supernatants were analyzed by size-exclusion high performance liquid chromatography (SEC). The supernatants of the samples were also analyzed on reducing SDS-PAGE with a 12% Tris-HCl ready gel (Bio-Rad).

Some samples were analyzed with SEC coupled with a triple detector (model 300TDA Detectors, Viscotek Co.), which monitors light scattering, refractive index, and intrinsic viscosity of proteins. Ovalbumin (Sigma A2512A, grade VI) was used for the calibration of the refractive index and light-scattering detectors and has a molecular mass of 42.7 kDa and refractive index increment with protein concentration (dn/dc) of 0.185 ml/g (31). Chromatograms were analyzed by the TriSEC 3.0 GPC software (Viscotek Co.) to determine molecular mass, radius of gyration (R_g), hydrodynamic radius (R_h), and intrinsic viscosity of the samples.

Circular Dichroism (CD) Spectroscopy—CD spectroscopy was performed with an Aviv 62DS spectrometer (Aviv) equipped with a Peltier temperature control unit. Far-UV CD spectra (190–260 nm) for 117 μM (2.97 mg/ml) SMA with various molar ratios of CR (r = 0, 1.2, 2.3, 4.8, and 8.8) were collected every 0.5 nm with an averaging time of 5 s at 25 °C in a 0.01-cm path length quartz cuvette. Near-UV CD spectra (260–340 nm) for 40 μM (1 mg/ml) SMA with various molar ratios of CR (r = 0, 1.3, 4.8, and 8.8) were collected every 0.5 nm with an averaging time of 5 s at 25 °C in a 0.1-cm path length quartz cuvette. The far- and near-UV CD spectra were collected immediately after mixing the samples.

To monitor protein aggregation directly in the sample cell, far-UV CD spectra of SMA (117 μM = 2.97 mg/ml) with various molar ratios of CR (r = 0, 1.3, 4.8, and 8.8) were acquired as described above during isothermal incubations at 37 °C (up to 140 min at 20-min intervals) and during heating from 25 to 60 °C at 5 °C intervals, with a dwell time of ≈25 min at each temperature. For the samples incubated isothermally at 37 °C for 140 min in the CD cell, the induced-CR CD spectrum (400–650 nm) was acquired at 37 °C every 1 nm with an averaging time of 5 s (14, 24, 25). The induced-CR CD spectrum (400–650 nm) was also collected at 37 °C for 40 μM native SMA and preformed amyloid fibrils of SMA in the presence of 160 μM CR.

For far- and near-UV CD spectra, raw spectra were corrected for the appropriate buffer blank and converted to mean residue ellipticity, [Θ] (deg cm^2/dmol) (32),

$$[\Theta] = \Theta_{obs} m_o / 10cl \quad \text{(Eq. 1)}$$

where Θ_{obs} is observed ellipticity in millidegrees, M_o is the mean residue molecular mass calculated from a molecular mass of 12.7 kDa and 108 residues (30), c is the protein concentration in mg/ml, and l is the path length of the quartz cell in cm.

Thermal unfolding of SMA (4 μM = 0.1 mg/ml) with various molar ratios of CR (r = 0, 1.3, 4.8, and 8.8) was studied by measuring ellipticity at 217 nm during heating from 25 to 80 °C at 1 °C intervals in a 0.1-cm path length cell with an averaging time of 5 s. Values for the midpoint of the transition region, T_m, for the unfolding curve for each sample were obtained as described before (6, 7).

Fourier Transform Infrared (FT-IR) Spectroscopy—IR spectra were acquired with a Bomem MB-104 FT-IR spectrometer equipped with a dTGS detector (6, 7). The spectra for 0.7 mM (16 mg/ml) SMA with various molar ratios of CR (r = 0, 1.3, and 2.8) were recorded at 25 °C in a liquid IR cell (P/N 20500, Specac Inc.) with CaF_2 windows separated by a 6-μm Mylar spacer (Chemplex Industries) (6, 7). Reference spectra for the appropriate buffer blank were recorded under identical scan conditions for the subtraction from the protein solution spectrum. Protein spectra were processed and analyzed as described previously (6, 7).

To monitor protein aggregation, IR spectra for 0.7 mM (16 mg/ml) SMA with various molar ratios of CR (r = 0, 1.3, and 2.8) were recorded at 37 °C as a function of time. The temperature was controlled by circulating ethylene glycol around a custom made IR cell holder and was measured by a thermal couple probe, inserted into a depression in the cell. Protein aggregation was monitored by following band intensity at 1627.8 cm^{-1} in the second derivative amide I spectra, which is indicative of intermolecular β-sheet (33, 34).

Hydrogen-deuterium exchange (HX) was initiated by mixing 1 volume of protein stock solution (1.6 mM = 40 mg/ml in H_2O buffer) with 3 volumes of 100% D_2O buffer containing an appropriate CR concentration to give a final protein concentration of 0.4 mM (10 mg/ml) SMA with various molar ratios of CR (r = 0, 0.02, 1.3, and 1.9) in 75% D_2O buffer. Samples were immediately placed in a liquid IR cell (P/N20500, Specac) with CaF_2 windows separated by a 12-μm polypropylene spacer (Chemplex Industries). A time-dependent series of spectra was acquired at 25 °C. The time from the sample preparation to acquisition of the first spectrum was about 90 s. HX was monitored by the shift in the frequency of the second derivative amide I band, which was at 1,639 cm^{-1} in spectra for the proteins in H_2O, as a function of the length of time of exposure to 75% D_2O buffer (6).

ThT Fluorescence Assay and Characterization of SMA Aggregates—The ThT fluorescence assay for the samples without CR was performed as described previously (6, 7). Samples with CR could not be analyzed by this method because of the absorbance of CR in the spectral region used for excitation of ThT. IR spectra were obtained to determine the secondary structure of the insoluble protein aggregates formed in the various conditions (6, 7). CR birefringence under crossed-polarization microscopy and transmission electron microscopy (TEM) of precipitated proteins were performed as described previously (6, 7). Precipitates formed without CR were stained with CR as described previously (29).

Isothermal Titration Calorimetry (ITC)—The thermodynamics of CR binding to SMA were measured using an isothermal titration microcalorimeter (VP-ITC, MicroCal Inc.) (35). The samples were thoroughly

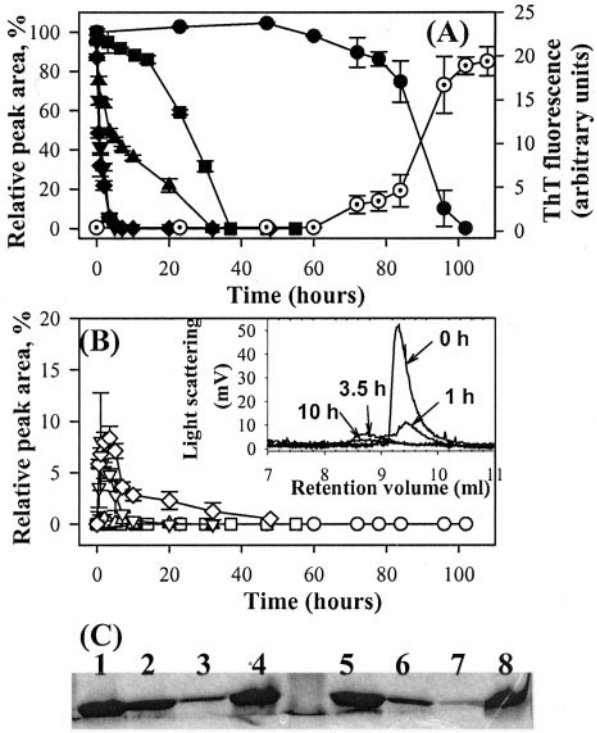

FIG. 1. Effects of CR on the levels of soluble native dimer (*A*) and non-native dimer species (*B*) of SMA during incubation at 37 °C with agitation in the presence of CR at r = 0 (●, ○), 0.3 (■, □), 1.3 (▲, △), 4.8 (▼, ▽), and 8.8 (♦, ◇). Data are shown as the percentage of the peak area in the SEC chromatogram relative to that for an unincubated control sample of 40 μM SMA dimer without CR. Also shown in *A* is the ThT fluorescence (⊙) for the SMA sample incubated without CR. The *inset* in *B* represents a light scattering signal for SMA samples incubated with CR at r = 8.8 for 0, 1, 3.5, and 10 h. *C*, reducing SDS-PAGE for supernatants of the samples incubated for 10 h (*lanes 1–4*) and 20 h (*lanes 5–8*). *Lanes 1* and *5*, CR at r = 0; *lanes 2* and *6*, CR at r = 1.3; *lanes 3* and *7*, CR at r = 4.8; *lanes 4* and *8*, CR at r = 8.8. *Errors bars* indicate the S.D. for triplicate samples.

degassed before each titration. The experiments were performed at 25 °C with 20.1 μM (0.5 mg/ml) SMA in the sample cell and 760 μM CR in the titrant syringe, at 25 °C with 32.3 μM (0.8 mg/ml) SMA and 1,036 μM CR, and at 30 °C with 20.1 μM (0.5 mg/ml) SMA and 760 μM CR. The sample in the cell was stirred at 300 rpm by the syringe, and 10 μl of titrant was delivered over 20 s with 180-s intervals between injections to allow complete equilibration. The data were collected automatically and subsequently analyzed by Origin software from MicroCal, Inc. Before the curve-fitting process, a background titration, consisting of the identical CR solution but only the buffer solution in the sample cell, was subtracted from each experimental titration to account for the heat of dilution (35). From the nonconstrained fitting to the plot of heat evolved/mol of CR injected *versus* the molar ratio of CR to SMA dimer, the binding stoichiometry (n), the binding enthalpy (ΔH), and the dissociation constant (K_d) were determined (35). The Gibbs free energy of binding (ΔG) was calculated by $\Delta G = -RT\ln(1/K_d)$. The entropy of binding ($T\Delta S$) was calculated by $T\Delta S = \Delta H - \Delta G$.

RESULTS

Effects of CR on Aggregation of SMA during Incubation at 37 °C with Agitation—Solutions of 40 μM (1 mg/ml) SMA with various molar ratios of CR (r = 0, 0.3, 1.3, 4.8, and 8.8) were incubated at 37 °C with agitation. The amount of soluble SMA remaining in solution was measured with SEC, as a function of incubation time (Fig. 1). Without CR, there was a lag phase during which soluble SMA levels did not decrease. After 3 days of incubation, there was a progressive loss of SMA from solution, with a concomitant increase of ThT fluorescence (Fig. 1). These results are characteristic of nucleation-dependent amyloid fibril formation kinetics (7). In the presence of CR, there was no apparent lag phase, and loss of soluble SMA was much faster, with the rate of loss increasing with increasing molar ratios (r) (Fig. 1). The SEC chromatograms showed no soluble oligomers for the samples with r = 0, 0.3, and 1.3 during the incubations.

Interestingly, in the chromatograms for samples with CR at r = 4.8 and 8.8, a new peak appeared before the elution of native dimer in samples incubated for ≥30 min (Fig. 1*B*, *inset*). To characterize further the protein molecules eluting at this time point, the SEC eluate was analyzed with Viscotek triple detectors that have light-scattering, refractive index, and viscosity instrumentation (31). The molecular mass values of the molecules in the early eluting and the native dimer peaks both were the same as that calculated for the native dimer (25.5 kDa), suggesting that the earlier peak may be the result of a non-native dimer species (Table I). R_g and R_h values for the putative non-native dimer species were about 20% greater than those for the native dimer, consistent with the degree of structural expansion characteristic of molten globules (36). Consistent with these observations, the non-native dimer species also had a greater intrinsic viscosity than the native dimer. However, the R_g/R_h ratio of both native and non-native dimer species was ~0.89, which is much closer to ~0.78 for compact spherical molecules than to ~1.5 for random coil structure (36, 37). Thus, the structurally expanded non-native dimer species maintains a spherical shape.

The level of non-native dimer species initially increased during incubation, concomitant with the loss of native SMA dimer. Then there was a gradual loss of the non-native dimer species, coinciding with the further reduction in the level of native SMA dimer (Fig. 1*B*). These results suggest that the non-native dimer species may be an intermediate on the aggregation pathway.

For samples with CR at r = 0, 0.3, 1.3 and 4.8, the loss of soluble SMA coincided with an increase of visible precipitated aggregates. In contrast, for samples with r = 8.8, there were no detectable precipitates until 20 h of incubation, even though soluble native SMA dimer was completely depleted after 5 h of incubation, and the non-native dimer species was populated after 30 min of incubation (Fig. 1). After 20 h, a small amount of precipitate (sufficient to account for about 10–20% of the total protein) was observed visually, but the precipitate amount did not increase during further incubation up to 4 days. To reconcile the inability to account for the loss of native protein caused by formation of non-native aggregates or precipitates, samples incubated for 10 and 20 h were centrifuged, and the supernatants were analyzed on reducing SDS-PAGE. As shown in Fig. 1*C*, the supernatants for samples with CR at r = 1.3 and 4.8 showed significant decreases in the amount of soluble SMA, consistent with SEC data. However, the supernatant for the sample with r = 8.8 showed an amount of protein similar to that of the sample for r = 0, which remained soluble without forming any aggregates for up to 3 days of incubation. So the majority of the protein in the incubated samples with CR at r = 8.8 remained soluble but appeared to interact with the SEC column, preventing detection in SEC analysis. Thus, the apparent loss of soluble protein indicated by the SEC analysis was caused by the formation of a soluble species that would not elute from the SEC column.

Real Time Measurements of SMA Aggregation by CD and IR Spectroscopies—To monitor structural changes of SMA during aggregation and determine the kinetics of aggregation, real time aggregation measurements were made with CD and IR spectroscopies. In studies with far-UV CD spectroscopy, solutions of 117 μM (2.97 mg/ml) SMA with various molar ratios of CR (r = 0. 1.3, 4.8, and 8.8) were incubated isothermally at 37 °C or heated from 25 to 60 °C (Fig. 2). Without CR, the

TABLE I

Physical and hydrodynamic parameters of native dimer and non-native dimer species of SMA determined by the SEC triple detector

Highly purified ovalbumin (Sigma, grade VI) was used for the calibration of light-scattering and refractive index detectors. The theoretical molecular mass of the SMA dimer is 25.5 kDa (30).

	Experimental molecular mass	Intrinsic viscosity	Radius of gyration (R_g)	Hydrodynamic radius (R_h)	R_g/R_h
	kDa	*dl/g*	*nm*	*nm*	
Native SMA dimer[a]	24.9 ± 0.4	0.018 ± 0.003	1.70 ± 0.01	1.90 ± 0.01	0.89 ± 0.01
Non-native dimer of SMA[a]	25.9 ± 0.9	0.026 ± 0.002	2.00 ± 0.05	2.24 ± 0.11	0.89 ± 0.05

[a] Means ± S.D. for three samples.

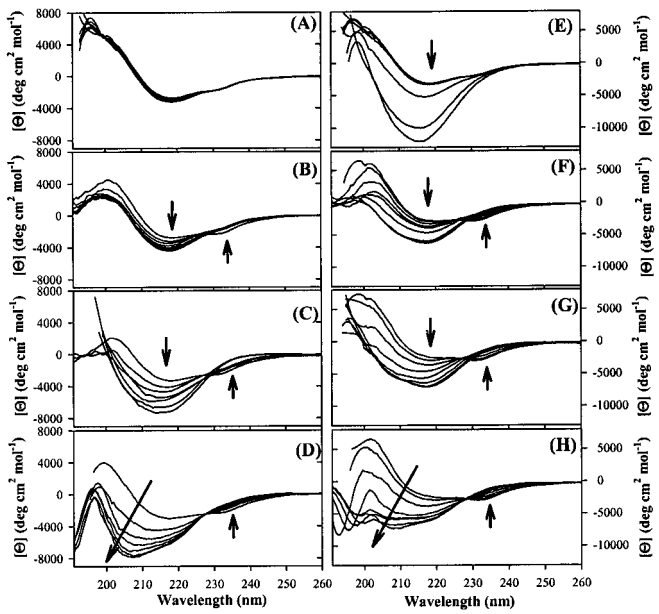

FIG. 2. **Effects of CR on far-UV CD spectra of SMA (117 μM) in the presence of CR at r = 0 (*A* and *E*), 1.3 (*B* and *F*), 4.8 (*C* and *G*), and 8.8 (*D* and *H*).** *A–D*, time-dependent spectra collected every 20 min during isothermal incubations at 37 °C for 140 min. *E–H*, temperature-dependent spectra collected every 5 °C during heating from 25 to 60 °C. *Arrows* indicate the spectral shifts with time or temperature increases.

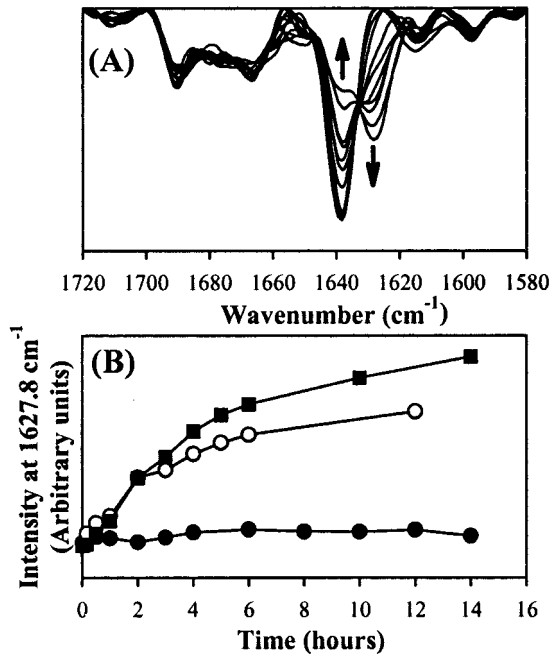

FIG. 3. **Effects of CR on IR spectra of SMA (0.7 mM) with CR at r = 0, 1.3, and 2.8 during incubation at 37 °C.** *A*, time course second derivative IR spectra of SMA with CR at r = 2.8, recorded at 0.015, 0.15, 0.5, 1, 2, 3, 4, 5, 6, 10, and 14 h. *Arrows* indicate the spectral shift with duration of incubation. *B*, time course intensity change at 1,627.8 cm^{-1} in second derivative IR spectra for SMA in the presence of CR at r = 0 (●), 1.3 (○), and 2.8 (■).

native secondary structure of SMA was not significantly changed by incubations up to 140 min at 37 °C (Fig. 2*A*) or by heating up to 45 °C (Fig. 2*E*). Secondary structure was rapidly lost during heating above 50 °C with large increases in negative ellipticity at 217 nm, which were most likely the result of non-native intermolecular β-sheets in protein aggregates (38). The short path length cell (0.01 cm) inhibited settling of insoluble aggregates on the time scale of the spectroscopic measurements (38). Aggregation of SMA at temperatures above 50 °C was expected because the onset temperature and T_m of thermal unfolding of SMA were 50 and 54 °C (see Fig. 9*B*), respectively.

Compared with results in the absence of CR, at r = 1.3 and 4.8 (Fig. 2, *B*, *C*, *F*, and *G*), the aggregation was much faster during isothermal incubation at 37 °C and occurred at lower temperatures during heating from 25 to 60 °C. The most rapid aggregation and the earliest onset temperature for aggregation were noted at r = 4.8. During isothermal incubation at 37 °C, the spectra indicated the presence of aggregates after 20 min. During heating, aggregates were noted at 30 °C. With CR at r = 8.8 in both isothermal and heating incubations, as time or temperature increased, the spectra gradually had increased negative ellipticity. The position of the minimum shifted to lower wavelengths, asymptotically approaching 205 nm (Fig. 2, *D* and *H*), which is close to the wavelength expected for unordered conformations (32).

Also, during far-UV CD experiments (Fig. 2), a negative CD band around 233 nm decreased in intensity as aggregation progressed in solutions with CR at r = 1.6 and 4.8, and unfolding progressed at r = 8.8. The negative band at 233 nm is contributed by aromatic residues, *i.e.* 2 Trp, 7 Tyr, and 2 Phe per monomer (30, 32, 39–41), consistent with studies on other proteins (42, 43). The spectra for the sample with CR at r = 8.8 showed a clear isosdichrotic point at 228 nm (Fig. 2, *D* and *H*), indicating a two-state unfolding process of SMA.

For the sample without CR, precipitates were visible after the completion of the thermal scan but not after isothermal incubation at 37 °C. In contrast, with CR at r = 1.3 and 4.8, precipitates were visible after incubations and thermal scans. Interestingly, with CR at r = 8.8, neither isothermal incubation nor thermal scans resulted in visible precipitates. Thus, in a solution of SMA with CR at r = 8.8, the combination of the dramatic structural changes evident in far-UV CD spectra, the absence of a intermolecular β-sheet signal at 217 nm, and the lack of visible precipitates suggest that SMA unfolded without aggregating.

Similar results were observed by FT-IR spectroscopy during isothermal incubations at 37 °C for 0.7 mM (16 mg/ml) SMA with CR at r = 0, 1.3, and 2.8 (Fig. 3). The second derivative IR spectra of native SMA without CR had a dominant band at 1639 cm^{-1}, indicating a predominance of β-sheet (29). During incubation at 37 °C in the absence of CR, there were no changes in the secondary structure of SMA during the 14 h of the experiment. With CR at r = 1.3 and 2.8, however, the native

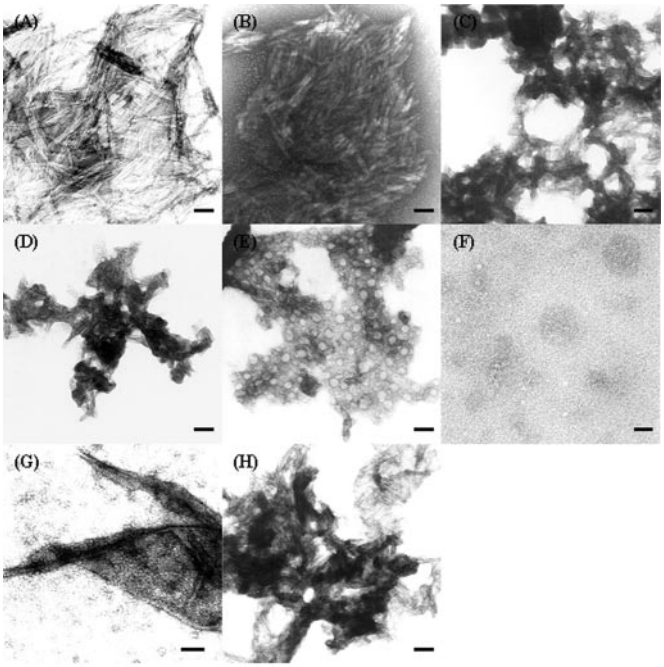

FIG. 4. **Representative TEM images for insoluble SMA aggregates.** *A–E*, images of SMA aggregates formed during incubation at 37 °C with agitation (Fig. 1) in the presence of CR at $r = 0$ for 103 h (*A*), $r = 0.3$ for 40 h (*B*), $r = 1.3$ for 40 h (*C*), $r = 4.8$ for 20 h (*D*), and $r = 8.8$ for 48 h (*E*). *F*, image of CR only (355 μM) after incubating at 37 °C with agitation for 48 h. *G* and *H*, images for insoluble aggregates formed during heating from 25 to 60 °C with CR at $r = 0$ (*G*) and $r = 1.3$ (*H*), under conditions identical to those used in the experiments for which results are given in Fig. 2, *A* and *B*, respectively. *Scale bars* represent 100 nm.

β-sheet structure of SMA gradually decreased, and a new band around 1,628 cm^{-1} grew in intensity, indicative of formation intermolecular β-sheet associated with protein aggregation (33, 34). The spectra showed an isosbestic point at 1,632.7 cm^{-1}, indicating two state-structural transitions of native SMA into the aggregates. The aggregation rate was faster for CR at $r = 2.8$ than at $r = 1.3$.

Characterization of the Aggregates—Precipitates formed during incubation at 37 °C with agitation (Fig. 1) were characterized by TEM, CR green birefringence, and FT-IR spectroscopy (Figs. 4–6). TEM images of the SMA aggregates formed with CR at $r = 0$ and 0.3 showed clumps of fibrils that were unbranched and ~8–12 nm in diameter (Fig. 4, *A* and *B*), which are typical of amyloid fibril morphology (2, 7). Further, CR staining of these samples showed strong green birefringence under polarized light (Fig. 5, *A–D*), which is also diagnostic of amyloid fibrils. TEM images of the SMA aggregates with CR at $r = 1.3$ and 4.8 showed mixed morphology with both fibrils and amorphous aggregates (Fig. 4, *C* and *D*), consistent with the reduced birefringence of CR-stained samples (Fig. 5, *E* and *F*; *cf*. Ref. 29). TEM images of the aggregates generated during thermal scans of SMA alone to 60 °C (Fig. 2*A*) also showed a mixed morphology of fibrils and amorphous aggregates (Fig. 4*G*). The TEM images of the precipitate formed in samples agitated at 37 °C with CR at $r = 8.8$ showed spherical structures with diameters of 20–34 nm (Fig. 4*E*). Similar and much larger (>150 nm) spheres were also observed for samples with CR only (Fig. 4*F*), which were generated under the same conditions used for incubating the SMA sample with CR at $r = 8.8$, (*i.e.* a 352 μM CR solution was incubated at 37 °C with agitation for 48 h). Thus the spheres most likely were CR micelles.

IR spectra of the precipitated SMA samples had dominant bands around 1,626–1,628 cm^{-1} and 1,689–1,693 cm^{-1} (Fig. 6), which are characteristic of non-native intermolecular anti-

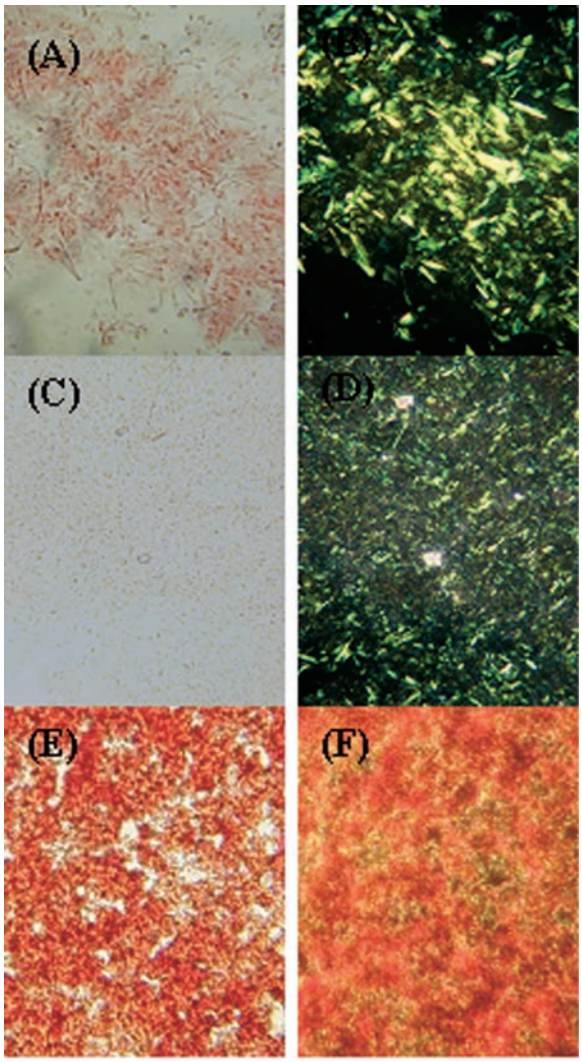

FIG. 5. **Representative images of CR staining and green birefringence of insoluble SMA aggregates formed during incubation at 37 °C with agitation in the presence of CR at $r = 0$ for 103 h (*A* and *B*), 0.3 for 40 h (*C* and *D*), 4.8 for 20 h (*E* and *F*) in the bright field (*A*, *C*, and *E*) and under cross-polarized light (*B*, *D*, and *F*).** Magnification, ×200.

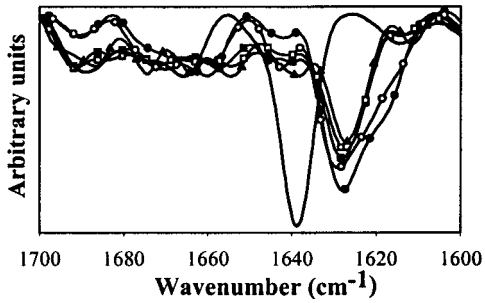

FIG. 6. **Second derivative IR spectra of the insoluble SMA aggregates formed during incubation at 37 °C with agitation (Fig. 1) in the presence of CR at $r = 0$ (●), 0.3 (○), 1.3 (■), 4.8 (□), and 8.8 (▲).** Also shown is the second derivative IR spectrum for the native SMA (*solid line*).

parallel β-sheet (6, 29, 33, 34). Minor differences between the spectra for precipitates formed in different levels of CR may be caused by differences in morphologies of the aggregates.

For the samples incubated isothermally at 37 °C for 140 min in the CD cell (Fig. 2, *A–D*), binding-induced CR CD spectra (400–650 nm) were collected to determine whether the aggre-

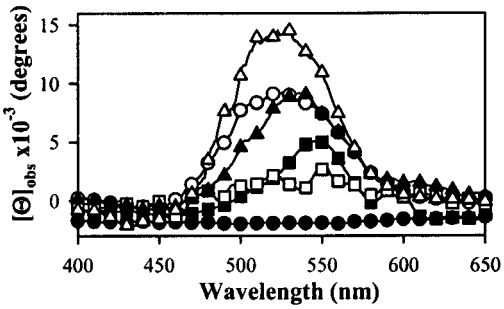

FIG. 7. **CD spectra of CR induced by binding to SMA aggregates formed during the incubations for which results are shown in Fig. 2, *B–D*.** Spectra are shown for samples with CR at r = 1.3 (□), 4.8 (▲), and 8.8 (△) after incubation at 37 °C for 140 min. Also shown are the induced CD spectra of CR in the presence of native SMA (with CR at r = 4.8, time = 0) (○), amyloid fibrils of SMA (■), and CR only (280 μM) (●).

gates contained amyloid fibrils (Fig. 7). The induced CD spectrum is caused by conformational changes of CR resulting from its binding to native proteins or amyloid fibrils (23–25). CR (Fig. 7) or protein alone (data not shown) did not show any optical activity in the 400–650 nm spectral region. Native SMA was mixed with CR and spectra acquired immediately. The spectrum showed a maximum peak around 530 nm, indicative of CR binding to SMA with distorted, nonsymmetric conformations (23–25). The spectrum of CR in the presence of SMA amyloid fibrils (generated by agitation at 37 °C for 4 days) had a maximum peak around 548 nm (Fig. 7), which is characteristic of the induced CD spectrum of CR upon binding to amyloid fibrils (14, 23). The aggregates formed during isothermal incubation with CR at r = 1.3 and 4.8 showed spectra with peak maxima close to 548 nm, indicating that the aggregates contained amyloid fibrils, consistent with the TEM results. However, in the spectrum for the SMA sample with CR at r = 8.8, the peak maximum was near 530 nm because SMA in this sample unfolded instead of forming fibrils (Fig. 7).

Effects of CR on the Secondary and Tertiary Structures of SMA—The stimulatory effects of CR on SMA amyloid fibril formation and aggregation prompted us to examine CR effects on secondary and tertiary structures of SMA at 25 °C, using far- and near-UV CD and IR spectroscopies (Fig. 8). The far-UV CD spectrum of native SMA without CR showed a negative band around 217 nm and a positive band around 200 nm, which are contributed by native β-sheet structure, as well as a negative band at 233 nm which is the result of aromatic residues, as discussed above. CR alone did not show any optical activity in the far-UV CD region (Fig. 8). The spectrum for denatured SMA in 4 M urea (7) had a minimum band around 204 nm, as expected for unordered conformations (32). In the spectra for native SMA in the presence of CR, the negative band around 233 nm gradually increased in intensity with increasing levels of CR, with an isosdichrotic point at 224 nm which is indicative of a two-state structural perturbation of the microenvironments of the aromatic residues. However, the β-sheet band at 217 nm was not altered in the presence of CR, indicating that CR does not greatly perturb the secondary structure of SMA. Similar results were obtained from second derivative IR spectra of SMA, which were minimally affected by CR at the ratios tested (Fig. 8*B*).

The near-UV CD spectrum of native SMA without CR showed positive maxima around 296 and 272 nm, a shoulder around 287 nm, and a minimum around 283 nm (Fig. 8*C*), consistent with previously reported results for SMA (41). A positive band at 296 nm has been ascribed to Trp and a negative band around 283 nm to Tyr (39–41). CR alone did not show

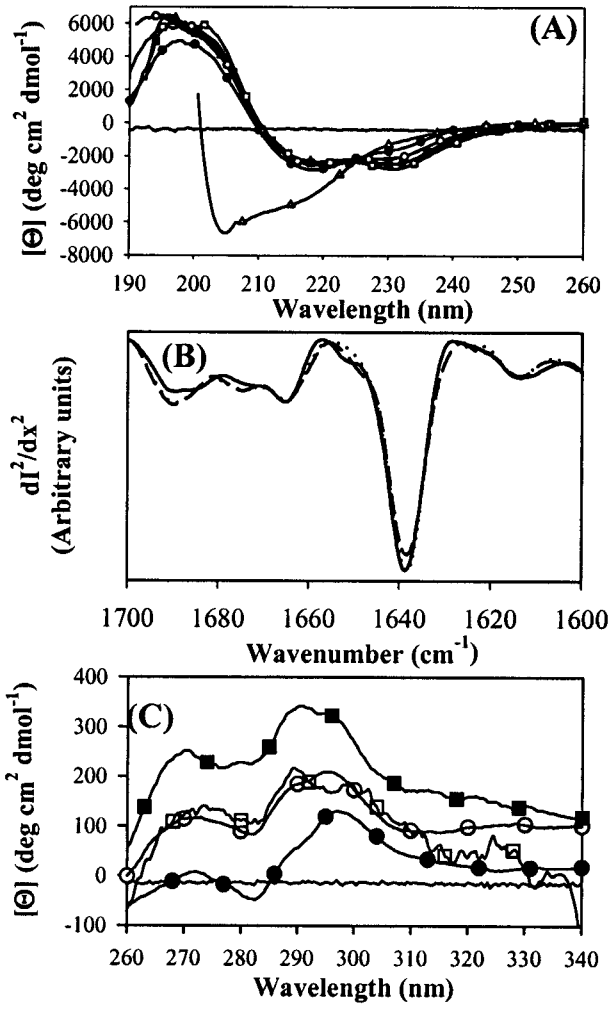

FIG. 8. **Effects of CR on the secondary and tertiary structures of SMA.** *A*, far-UV CD spectra of SMA in the presence of CR at r = 0 (●), 1.2 (○), 2.3 (■), 4.8 (□), and 8.8 (▲) at 25 °C. Also shown is the spectrum for SMA incubated overnight in 4 M urea (△) and for CR (280 μM) buffer only (*solid line*). *B*, second derivative IR spectra of SMA (0.7 mM) with r = 0 (*solid line*), r = 1.3 (*dotted line*), and r = 2.8 (*dashed line*) at 25 °C. *C*, near-UV CD spectra of SMA with r = 0 (●), 1.3 (○), 4.8 (■), and 8.8 (□) at 25 °C. Also shown is the spectrum for CR only (280 μM) (*solid line*).

any optical activity (Fig. 8*C*). In the spectra for SMA in the presence of CR, the peaks around 296, 283, and 272 nm were gradually blue shifted with increasing levels of CR, indicating CR-induced solvent exposure of aromatic groups in the protein (39, 40).

Taken together, the far-UV CD, near-UV CD, and IR spectroscopic results documented that CR perturbed the tertiary structure of native SMA without significantly affecting the secondary structure of the protein. It is important to note that these spectroscopic studies were conducted at 25 °C, and the spectra do not show any signal (*e.g.* because of non-native β-sheet or light scattering) indicative of protein aggregates.

Effects of CR on the Thermal Stability and HX of SMA—Thermal unfolding of SMA (4 μM = 0.1 mg/ml) was studied with far-UV CD spectroscopy at various molar ratios of CR (r = 0, 1.3, 4.8, and 8.8) (Fig. 9, *A* and *B*). Far-UV CD spectra of all samples at 80 °C showed a negative maximum centered at about 205 nm (Fig. 9*A*), indicating that thermal unfolding rather than aggregation occurred at the relatively low protein concentration used in these experiments. The thermal unfolding was irreversible. The T_m values were 53.9 ± 0.3 °C for SMA alone, 47.0 ± 0.5 °C for r = 1.3, 43.9 ± 0.4 °C for r = 4.8, and

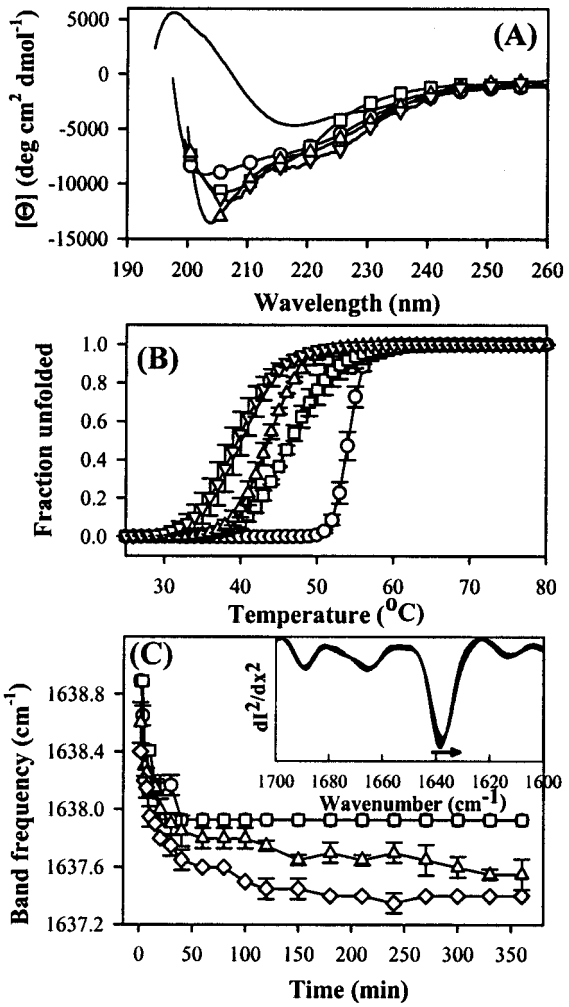

FIG. 9. **Effects of CR on thermal stability and HX of SMA.** *A*, far-UV CD spectra of SMA (4 μM) collected at 80 °C in the presence of CR at r = 0 (○), 1.3 (□), 4.8 (△), and 8.8 (▽). Also shown is the spectrum for SMA (4 μM) in buffer only at 25 °C before heating (*solid line*). *B*, fraction of unfolded SMA as a function of temperature in the presence of CR at r = 0 (○), 1.3 (□), 4.8 (△), and 8.8 (▽). *C*, HX rates of SMA in the presence of CR at r = 0 (○), 0.02 (□), 1.3 (△), and 1.9 (◇). HX was monitored by the shift in band frequency around 1,638 cm^{-1} as a function of the length of time of exposure to 75% D_2O buffer. *Inset*, changes in second derivative amide I IR spectrum of SMA in the presence of CR at r = 1.9 as a function of the length of time of exposure to 75% D_2O buffer. The *arrow* indicates the direction of time-dependent spectral shifts. *Errors bars* indicate the S.D. for duplicate samples.

39.5 ± 1.6 °C for r = 8.8, showing that CR lowered the thermal stability of SMA (Fig. 9*B*).

The HX of SMA (400 μM = 10 mg/ml) was measured in real time with FT-IR spectroscopy at 25 °C, in solutions with various molar ratios of CR (r = 0, 0.02, 1.3, and 1.9) (Fig. 9*C*). During the 6-h HX experiment, all SMA samples maintained native secondary structure (Fig. 9*C*, *inset*). During HX, there was a time-dependent shift in the position of the major β-sheet band at about 1,638 cm^{-1}. The rate at which HX occurred was faster in the presence than in the absence of CR (Fig. 9*C*).

Thermodynamics of CR Binding to SMA Measured by ITC—Fig. 10 shows representative data from ITC for a titration of CR to SMA at 25 °C. The CR titration to buffer only was endothermic with greater heat absorption in the initial injections (Fig. 10*A*). CR readily forms self-assembled micelle-like structures in water at high ionic strength or above 5 μM at physiological pH (24, 25), but monomeric CR may also exist transiently (44). The initial larger endothermic peaks presumably were caused

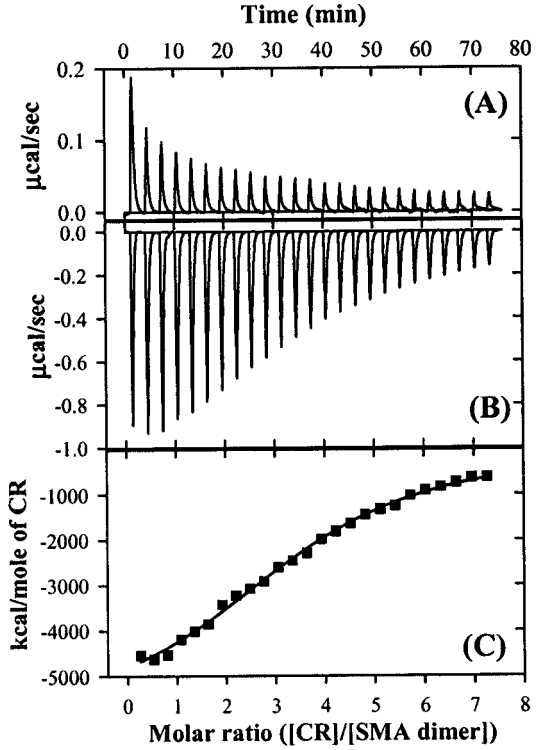

FIG. 10. **Representative ITC data analysis for titration of CR (760 μM titrant concentration) into buffer (*A*) and into a solution of 20.1 μM SMA dimer (*B* and *C*) at 25 °C.** Titrations consisted of 25 injections (10 μl each) of CR. *A* and *B* show the raw heat data as a function of injection number, and *C* shows enthalpy changes as a function of molar ratios of CR to SMA dimer.

by the dissociation of CR from micelles during dilution in the reaction cell, an effect that decreased with further injections because the dilution of CR was decreased (45).

CR titrations to SMA were exothermic (Fig. 10*B*). The enthalpy change as a function of the molar ratios of CR to SMA dimer increased without a clear inflection point (Fig. 10*C*). The results were fit best with a model in which binding to each site has equal energy, using Origin software supplied by MicroCal, Inc. The binding stoichiometry (n) was about 3.4 at 25 °C and 5.1 at 30 °C. K_d values were in the μM range, showing that the binding between CR and SMA is relatively strong (35, 46). The enthalpic contribution to the free energy of binding was dominant (Table II). After the titration experiments, samples were removed from the cell and analyzed by SEC. Aggregates were not detected in samples titrated at 25 or 30 °C (data not shown). In contrast, when titrations were conducted at 37 °C, soluble oligomers were formed (data not shown), precluding the use of these data to calculate binding parameters.

DISCUSSION

Interactions of CR with SMA—The binding molar ratios of CR molecules/SMA dimer increased from ~3.4 at 25 °C to ~5 at 30 °C. The increased binding at higher temperature is likely the result of exposure of new binding sites on the protein as temperature increases. A previous study also showed that the binding molar ratios of CR molecules to a λ-type V_L dimer were ~8 at 40–45 °C and ~16 at 55 °C, measured by gel extraction analysis (22). The dissociation constant (~19 μM) of CR binding to SMA is similar to that (~9 μM) of CR binding to Aβ-amyloid fibrils determined by filtration method using radiolabeled CR (47).

Even though CR has been shown to bind to several proteins (9, 14, 22–28), the main binding interactions still remain controversial. The structural features of CR suggest that the bind-

TABLE II
Thermodynamic parameters for the interactions between SMA and CR measured by ITC
Values are the mean ± S.D. from two or three experiments.

Temperature	[SMA dimer]	[CR]	n [CR]/[SMA dimer]	K_d	ΔG^a	ΔH	$T\Delta S^b$
°C	*μM*	*μM*		*μM*	*kcal/mol*	*kcal/mol*	*kcal/mol*
25	20.1	760	3.6 ± 0.1	17 ± 1	−6.5 ± 0.1	−5.9 ± 0.1	0.7 ± 0.2
25	32.3	1036	3.3 ± 0.0	21 ± 1	−6.4 ± 0.1	−6.5 ± 0.2	−0.1 ± 0.2
30	20.1	760	5.1 ± 0.4	34 ± 6	−6.1 ± 0.1	−5.4 ± 0.7	0.7 ± 0.5

[a] Calculated by $\Delta G = -RT\ln(1/K_d)$.
[b] Calculated by $T\Delta S = \Delta H - \Delta G$.

ing most likely occurs through hydrophobic interactions, electrostatic interactions, or both. Some earlier studies proposed that binding occurs through hydrophobic interactions between the biphenyl rings of CR and hydrophobic pockets and clefts on proteins (14, 17, 22, 48). However, our ITC data showed that the formation of a CR·SMA complex was dominantly enthalpically driven, excluding hydrophobic interactions (35, 46). Hydrophobic interactions are characterized mainly by small enthalpy changes and large positive entropy changes, resulting from the release into the bulk solution of relatively highly ordered water molecules that surround the hydrophobic surfaces of two interacting molecules (35, 46). Further, the observed decrease in the magnitude of negative enthalpy with increased temperature (Table II) is opposite the phenomenon associated with the burial of solvent-accessible hydrophobic surfaces (35, 46). Thus it seems that the electrostatic interactions between the sulfate groups of CR and the positively charged residues of SMA are responsible for the formation of a CR·SMA complex. Previous studies also showed that electrostatic interactions were responsible for the binding of CR to Aβ-peptides (27), prion proteins (9, 10), and β_2-microglobulin, which is a structural homolog of V_L (28), indicating that the sulfate groups of CR are important for its binding to proteins.

Effects of CR on Aggregation and Conformation of SMA—With CR at $r = 0.3$, 1.3, 4.8, aggregation of SMA was greatly accelerated (Figs. 1–3), and the resulting aggregates and fibrils had a non-native intermolecular β-sheet structure that is typical of amyloid fibrils and protein precipitates. Accelerated aggregation was associated with binding of CR to the protein, which reduced the thermal stability of SMA and greatly favored SMA species with perturbed tertiary structure and native secondary structure (*i.e.* molten globules). Our HX results also indicated that in the presence of CR, the molecular population of SMA was shifted toward partially unfolded species, which are highly reactive to aggregation (1, 3, 6, 49). Previous studies showed that CR stabilized the molten globule-like states of IgG molecules and a λ-light chain dimer (26, 50). A similar amphipathic dye, 8-anilino-1-naphthalenesulfonate (ANS), also favored a partially folded conformation of pectate lyase C (51).

As can be shown through application of the Wyman linkage function (52), preferential binding of CR and ANS to partially unfolded protein molecules shifts the equilibrium between protein substates toward these species. Because the partially unfolded molecules are aggregation-competent, ligand binding greatly accelerates protein aggregation. This effect of ligands contrasts with the inhibition of protein aggregation which can be realized with ligands that bind strongly with the fully native protein conformation (8). In this case, the same Wyman linkage function describes how ligand binding shifts the equilibrium toward the native state and away from aggregation-competent, partially unfolded species.

CR binds to partially folded SMA with a stoichiometry of about 4 mol of CR/mol of SMA dimer. At higher CR concentrations (*e.g.* $r = 8.8$), CR binds to denatured SMA molecules, favoring their population. Protein aggregation occurs through partially unfolded molecules and not from the fully unfolded state (1, 3, 49). High concentrations of CR reduce aggregation (Figs. 1 and 2) by populating the denatured state of SMA.

Thus, the overall effect of CR binding on protein aggregation depends on the concentrations of CR and protein, which dictate the amount of CR bound and hence the equilibrium between protein species. At lower concentrations CR binds to and populates partially unfolded forms of SMA, which accelerates aggregation. In contrast, higher concentrations of CR favor unfolding of SMA, and, hence, result in reduced aggregation. These concentration-dependent effects of CR on protein aggregation resemble those of chaotropes such as urea and guanidine hydrochloride. Previous studies have shown that at relatively low concentrations, these denaturants populated partially unfolded protein molecules and foster aggregation, whereas at higher concentration they greatly favor the unfolded state and thus prevent aggregation (5, 53).

These insights can be used to reconcile the apparently conflicting results from earlier reports on the effects of CR on protein aggregation and fibril formation. At high molar ratios of CR to the protein, *e.g.* $r \geq 60$ for prion protein (9, 10, 12) and $r \geq 300$ for Aβ-peptides (13, 20), amyloid fibril formation by these proteins was inhibited. In contrast, at lower molar ratios CR accelerated fibril formation from Aβ-peptides (13) and prion proteins (12). Although the detailed mechanism by which CR operates in a dose-dependent manner remains to be established for these and other proteins, we speculate that at relatively low concentrations, CR binding populates partially folded, aggregation-competent species of the proteins. At higher concentrations, CR inhibits fibril formation because it favors the denatured state, which is much less prone to aggregate.

It has been suggested previously that CR inhibits fibril formation by prion proteins by stabilizing the so-called "scrapie" conformation to such a high degree that further unfolding, which is thought to be required for this conformation to assemble into fibrils, is inhibited (54). It also has been proposed that CR inhibits fibril formation by blocking binding sites for other molecules that are promoters of protein aggregation (48). However, neither of these mechanisms can account for the concentration-dependent effects of CR on protein aggregation and fibrillogenesis.

The dose-dependent effects of CR binding on protein conformational equilibria have implications for practical therapeutic use of CR or its analogs. During dosing to obtain the high level of CR potentially needed to inhibit amyloid fibril formation, there would be periods of time during which lower concentrations of CR were present. The lower concentration of CR could induce fibril formation. Thus CR or its analogs could cause increased rather than decreased pathology.

Biological Implications—CR has two anionic sulfate groups and in that respect resembles the sulfated glycosaminoglycans (GAGs), which are the main components of basement mem-

brane glycoproteins (*e.g.* heparan sulfate, chondroitin sulfate, and demartan sulfate) and *in vivo* frequently deposit coincidentally with amyloid fibrils of a variety of proteins including Aβ-peptides, prions, serum amyloid A, and immunoglobulin light chains (55). Interestingly, sulfated GAGs stimulate amyloid fibril formation by Aβ-peptides and α-synuclein *in vitro* (56–58), suggesting that they could enhance amyloid fibril formation *in vivo*. CR competes with sulfated GAGs for binding with prion proteins, suggesting that they bind to same sites, most likely through sulfates (9). A previous study showed that several V_L's, including SMA, interact with GAGs by electrostatic interactions between the sulfate groups of GAGs and the positively charged residues of the proteins (59). These interactions may be responsible for the enhanced fibrillogenesis of proteins in the presence of GAGs which, analogously to CR, may favor population of partially unfolded, aggregation competent protein species.

CONCLUSIONS

The concentration-dependent effects of CR on SMA aggregation and fibril formation depend on which protein species is favored upon binding of this ligand. For any given ligand, its effect on amyloid fibril formation will similarly be dictated by how its binding affects the equilibrium between protein species. Thus, in efforts to discover potential therapeutic compounds for inhibition of amyloidosis, it is important that *in vitro* screening studies take into account not only the binding affinity of the ligands for the target protein, but also the effect of binding on the molecular population of the protein. In addition, concentration-dependent effects of compounds on both amyloid fibril formation and protein structure should be studied in these screening efforts.

Acknowledgments—We greatly appreciate the Biophysics Core Facility at the Biomolecular Structure Program for access to the ITC instrument. We thank Dot Dill for help with TEM, Prof. Judith Snyder at the University of Denver for use of polarization microscopy, and Prof. Robert Woody at Colorado State University and Dr. Barbara Piekarska at Collegium Medicum Jagiellonian University in Poland for helpful communications.

REFERENCES

1. Kelly, J. W. (1996) *Curr. Opin. Struct. Biol.* **6,** 11–17
2. Serpell, L. C., Sunde, M., and Blake, C. C. F. (1997) *Cell. Mol. Life Sci.* **53,** 871–887
3. Fink, A. L. (1998) *Fold. Des.* **3,** R9–R23
4. Hurle, M. R., Helms, L. R., Li, L., Chan, W., and Wetzel, R. (1994) *Proc. Natl. Acad. Sci. U. S. A.* **91,** 5446–5450
5. Raffen, R., Dieckman, L. J., Szpunar, M., Wunschl, C., Phani, R. P., Poras, D., Wilkens-Stevens, P., Cai, X., Schiffer, M., and Stevens, F. J. (1999) *Protein Sci.* **8,** 509–517
6. Kim, Y.-S., Wall, J. S., Meyer, J., Murphy, C., Randolph, T. W., Manning, M. C., Solomon, A., and Carpenter, J. F. (2000) *J. Biol. Chem.* **275,** 1570–1574
7. Kim, Y.-S., Cape, S. P., Chi, E., Raffen, R., Wilkins-Stevens, P., Stevens, F. J., Manning, M. C., Randolph, T. W., Solomon, A., and Carpenter, J. F. (2001) *J. Biol. Chem.* **276,** 1626–1633
8. Miroy, G. J., Lai, Z., Lashuel, H. A., Peterson, S. A., Strang, C., and Kelly, J. W. (1996) *Proc. Natl. Acad. Sci. U. S. A.* **93,** 15051–15056
9. Caughey, B., Brown, K., Raymond, G. J., Katzenstein, G. E., and Thresher, W. (1994) *J. Virol.* **68,** 2135–2141
10. Demaimay, R., Harper, J., Gordon, H., Weaver, D., Chesebro, B., and Caughey, B. (1998) *J. Neurochem.* **71,** 2534–2541
11. Findeis, M. A. (2000) *Biochim. Biophys. Acta* **1502,** 76–84
12. Rudyk, H., Vasiljevic, S., Hennion, R. M., Birkett, C. R., Hope, J., and Gilbert, I. H. (2000) *J. Gen. Virol.* **81,** 1155–1164
13. Esler, W. P., Stimson, E. R., Ghilardi, J. R., Felix, A. M., Lu, Y.-A., Vinters, H. V., Mantyh, P. W., and Maggio, J. E. (1997) *Nat. Biotechnol.* **15,** 258–263
14. Benditt, E. P., Eriksen, N., and Berglund, C. (1970) *Proc. Natl. Acad. Sci. U. S. A.* **66,** 1044–1051
15. Glenner, G. G. (1980) *N. Engl. J. Med.* **302,** 1283–1292
16. Klunk, W. E., Jacob, R. F., and Mason, R. P. (1999) *Methods Enzymol.* **309,** 285–305
17. Turnell, W. G., and Finch, J. T. (1992) *J. Mol. Biol.* **227,** 1205–1223
18. Roterman, I., Król, M., Nowak, M., Konieczny, L., Rybarska, J., Stopa, B., Piekarska, B., and Zemanek, G. (2001) *Med. Sci. Monit.* **7,** 771–784
19. Klunk, W. E., Debanth, M. L., and Pettegrew, J. W. (1994) *Neurobiol. Aging* **15,** 691–698
20. Podlisny, M. B., Walsh, D. M., Amarante, P., Ostaszewski, B. L., Stimson, E. R., Maggio, J. E., Teplow, D. B., and Selkoe, D. J. (1998) *Biochemistry* **37,** 3602–3611
21. Lorenzo, A., and Yankner, B. A. (1994) *Proc. Natl. Acad. Sci. U. S. A.* **91,** 12243–12247
22. Piekarska, B., Konieczny, L., Rybarska, J., Stopa, B., Zemanek, G., Szneler, E., Krol, M., Nowak, M., and Roterman, I. (2001) *Biopolymers* **59,** 446–456
23. Khurana, R., Uversky, V. N., Nielsen, L., and Fink, A. L. (2001) *J. Biol. Chem.* **276,** 22715–22721
24. Edwards, R. A., and Woody, R. W. (1977) *Biochem. Biophys. Res. Commun.* **79,** 470–476
25. Woody, A.-Y. M., Reisbig, R. R., and Woody, R. W. (1981) *Biochim. Biophys. Acta* **655,** 82–88
26. Piekarska, B., Roterman, I., Robarska, J., Koniczny, L., and Kaszuba, J. (1994) *J. Physiol. Pharmacol.* **45,** 147–162
27. Inouye, H., Nguyen, J. T., Fraser, P. E., Shinchuk, L. M., Packard, A. B., and Kirschner, D. A. (2000) *Amyloid* **7,** 179–188
28. Heegaard, N. H. H., Sen, J. W., and Nissen, M. H. (2000) *J. Chromatogr. A* **894,** 319–327
29. Kim, Y.-S., Randolph, T. W., Stevens, F. J., and Carpenter, J. F. (2002) *J. Biol. Chem.* **277,** 27240–27246
30. Wilkins-Stevens, P., Raffen, R., Hanson, D. K., Deng, Y.-L., Berrios-Hammond, M., Westholm, F. A., Murphy, C., Eulitz, M., Wetzel, R., Solomon, A., Schiffer, M., and Stevens, F. J. (1995) *Protein Sci.* **4,** 421–432
31. Wen, J., Arakawa, T., and Philo, J. S. (1996) *Anal. Biochem.* **240,** 155–166
32. Woody, R. W. (1995) *Methods Enzymol.* **246,** 34–71
33. Dong, A., Prestrelski, S. J., Allison, S. D., and Carpenter, J. F. (1995) *J. Pharm. Sci.* **84,** 415–424
34. Kendrick, B. S., Cleland, J. L., Lam, X., Nguyen, T., Randolph, T. W., Manning, M. C., and Carpenter, J. F. (1998) *J. Pharm. Sci.* **87,** 1069–1076
35. Wiseman, T., Williston, S., Brandts, J. F., and Lin, L.-N. (1989) *Anal. Biochem.* **179,** 131–137
36. Ptitsyn, O. B. (1992) in *Protein Folding* (Creighton, T. E., ed) pp. 243–300, Freeman, New York
37. Oono, Y., and Kohmoto, M (1983) *J. Chem. Phys.* **78,** 520–528
38. Matsuura, J. E., and Manning, M. C. (1994) *J. Agric. Food Chem.* **42,** 1650–1656
39. Strickland, E. H. (1974) *CRC Crit. Rev. Biochem.* **2,** 113–175
40. Woody, R. W., and Dunker, A. K. (1996) in *Circular Dichroism and the Conformational Analysis of Biomolecules* (Fasman, G. D., ed) pp. 109–157, Plenum Press, New York
41. Khurana, R., Gillespie, J. R., Talapatra, A., Minert, L. J., Ionescu-Zanetti, C., Millett, I., and Fink, A. L. (2001) *Biochemistry* **40,** 3525–3535
42. Vuilleumier, S., Sancho, J., Loewenthal, R., and Fersht, A. R. (1993) *Biochemistry* **32,** 10303–10313
43. Freskagård, P.-O., Mårtensson, L.-G., Jonasson, P., Johnsson, B.-H., and Carlsson, U. (1994) *Biochemistry* **33,** 14281–14288
44. Skowronek, M., Stopa, B., Konieczny, L., Rybarska, J., Piekarska, B., Szneler, E., Bakalarski, G., and Roterman, I. (1998) *Biopolymers* **46,** 267–281
45. Bijma, K., Rank, E., and Engberts, J. B. F. N. (1998) *J. Colloid. Interface Sci.* **205,** 245–256
46. Holdgate, G. A. (2001) *BioTechniques* **31,** 164–184
47. Ashburn, T. T., Han, H., McGuinness, B. F., and Lansbury, P. T., Jr. (1996) *Chem. Biol.* **3,** 351–358
48. Kuner, P., Bohrmann, B., Tjernberg, L. O., Nalund, J., Huber, G., Celenk, S., Grüninger-Leitch, F., Richard, J. G., Jakob-Roethne, Kemp, J. A., and Nordsted, C. (2000) *J. Biol. Chem.* **275,** 1673–1678
49. Speed, M. A., Wang, D. I., and King, J. (1996) *Nat. Biotechnol.* **14,** 1283–1287
50. Piekarska, B., Skowronek, M., Rybarska, J., Stopa, B., Roterman, I., and Konieczny, L. (1996) *Biochimie* (*Paris*) **78,** 183–189
51. Kamen, D. E., and Woody, R. W. (2001) *Protein Sci.* **10,** 2123–2130
52. Wyman, J., and Gill, S. T. (1991) *Binding and Linkage: Functional Chemistry of Macromolecules*, University Science Books, Mill Valley, CA
53. De Young, L. R., Dill, K. A., and Fink, A. L. (1993) *Biochemistry* **32,** 3877–3886
54. Caspi, S., Halimi, M., Yanai, A., Sasson, S. B., Taraboulos, A., and Gabizon, R. (1998) *J. Biol. Chem.* **273,** 3484–3489
55. Kisilevsky, R. (2000) *J. Struct. Biol.* **130,** 99–108
56. Fraser, P. E., Nguyen, J. T., Chin, D. T., and Kirschner, D. A. (1992) *J. Neurochem.* **59,** 1531–1540
57. Castillo, G. M., Lukito, W., Wight, T. N., and Snow, A. D. (1999) *J. Neurochem.* **72,** 1681–1687
58. Cohlberg, J. A., Li, J., Uversky, V. N., and Fink, A. L. (2002) *Biochemistry* **41,** 1502–1511
59. Jiang, X., Myatt, E., Lykos, P., and Stevens, F. J. (1997) *Biochemistry* **36,** 13187–13194